Journal of Materials Chemistry A

Accepted Manuscript

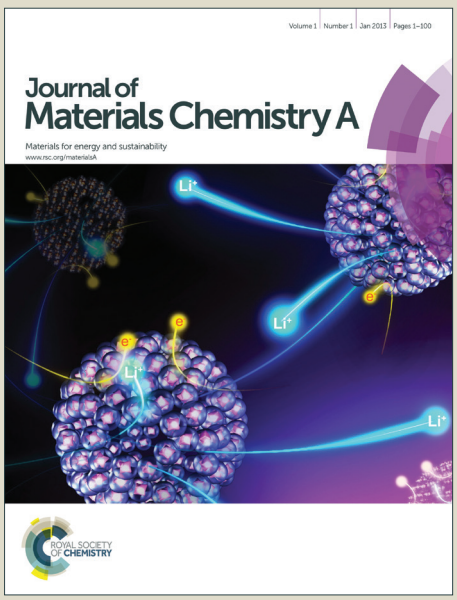

ROYAL SOCIETY OF CHEMISTRY

www.rsc.org/materialsA

Hierarchical Rough Surfaces Formed by LBL Self-assembly for Oil/Water Separation

Xiaoyu Li,[a] Dan Hu,[a,b] Kun Huang,[a] and Chuanfang Yang[a,*]

[a] *Key Laboratory of Green Process and Engineering, Institute of Process Engineering, Chinese Academy of Sciences, Beijing 100190, China*

[b] *University of Chinese Academy of Sciences, Beijing 100049, China*

** Corresponding author.*

Tel/Fax: +86 10 82544976. E-mail: cfyang@ipe.ac.cn

Abstract: Controlled assembly of nano-scale building units to form special micro/nano structures is of interest for achieving desired properties in many practical applications. The raspberry or strawberry-like hierarchical structure with multi-level dimension is one of the examples for special surface wettability design. In this work, a series of coatings with hierarchical nanostructure and dual roughness are constructed on sintered stainless steel mesh and stainless steel fiber felt via layer-by-layer (LBL) self-assembly of SiO_2 nanoparticles (NPs) having different sizes. The surface is then chemically treated to gain the needed wetting properties for intended separation of oil from water. The surface morphology of the coatings is observed using scanning electron microscopy (SEM) and atom force microscopy (AFM). The surface wetting properties are investigated by measuring the coatings' water and oil contact angle (WCA and OCA) in air and under water. The results show that the stainless steel mesh with such coatings having superhydrophobicity, and thus can efficiently separate

regular oil/water mixtures. Furthermore, the stainless steel fiber felt treated with similar coatings can also separate oil-in-water emulsions through the non-sieving coalescence mechanism, achieving an oil/water separation efficiency as high as 99.4%.

Keywords: Stainlesss steel mesh/felt; Hierarchical nanostructure; Self-assembly; Wettability; oil/water separation

1. Introduction

Oil/water separation is a global challenge because of tougher regulations of oily industrial wastewater discharge, the need of water recycle and reuse, as well as frequent crude oil leakage.[1-3] Moreover, emulsified-oil containing wastewater generated in daily lives and many industrial processes, such as textile, leather, petrochemical, food, steel and metal finishing, is much more difficult to treat than that of regular oil/water mixtures, the direct release of which will undoubtedly bring about harm to the environment and people's health.[4-5] Traditional techniques for oil/water separation such as air flotation, gravity separation combined with skimming, oil absorbing, coalescence and flocculation are often limited by low separation efficiencies, especially for tiny oil droplets,[6-9] high energy-cost, and complex separation instruments. The use of membrane technology such as microfiltration and ultrafiltration is very advantageous in terms of membrane's high emulsion separation efficiency, but membrane fouling is a persistent problem to be concerned with. In addition, polymeric membranes may not be able to withstand the harsh operation conditions that often require high flow, the ability to process particulates, the ability to resist acidity and the material's compatibility with oils. Moreover, energy cost because of the very high pumping power needed for membrane operation is always a big issue. Encouragingly, some recently reported membrane-oriented technologies based on sieving principle for the separation exhibited promising potentials for energy-saving, easy and efficient removal of oil from water, and even emulsified

oil/water mixtures.[10-14] However, these preliminary techniques are still in infant stage, more explorations such as the choice of membranes, facile membrane modifications, and suitable selection of modifying materials, are thus needed.[15-17]

It was well documented that the introduction of superhydrophobicity can effectively achieve or improve oil/water separation efficiency.[18-24] Since surface wettability can be tuned by controlling surface chemistry and surface roughness, various super-hydrophobic surfaces and films have been prepared by adjusting these two parameters.[25-28] Despite these pioneering work, an inexpensive and broadly applicable approach towards designing super-wetting coalescence materials for effective separation of various oil/water mixtures, especially oil-in-water emulsions, is highly desired. Besides, a demand for rationally designing the pore size distribution of a material that provides a comprehensive performance with good mechanical strength, the ability for repeated use and long-term preservation, is also seen for emulsion separation practically.

Until now, various approaches have been developed to achieve the controllable surface roughness, including chemical etching, electrochemical deposition, sputtering, sol–gel process, layer-by-layer (LBL) assembly and so on.[29-36] Among them, the LBL assembly provides an environmentally benign, and inexpensive way for both design and fabrication of particle coatings with tailored chemical composition and controllable architecture on substrate surfaces. This bottom-up approach is also an ideal way for preparation of multifunctional particle coatings.[37-39] Compared with sol-gel or sputtering process, it can easily control the coating thickness at the nanoscale level, and the thin coatings do not change the macro-morphology of the substrate materials. However, few particle coatings were fabricated on fibers or meshes using this approach for effective oil/water emulsion separation.

Here, via LBL method using SiO_2 NPs with different sizes, we successfully constructed a series of nanoparticle (NP) coatings with hierarchical raspberry-like nanostructure and dual-roughness on sintered stainless steel mesh and sintered stainless steel fiber felt. We chose stainless steel mesh and felt because they are robust filter materials alone that can endure many harsh field conditions. The resultant mesh

after chemical surface modification exhibited superhydrophobicity, and thus achieving high separation efficiency for regular oil/water mixtures. What is more interesting is that, the felt with similar coatings can effectively separate oil-in-water emulsions with an efficiency of up to 99.4%, through coalescence instead of sieving mechanism. Another advantage of using the felt is its ability to allow for high fluid flow and minimize fouling while conducting the separation, attributed to its micron-meter level pore size on the order of 1-10 μm.

2. Experimental Section

Materials: Tetraethyl orthosilicate (TEOS, 99+ %) was obtained from Alfa Aesar. Poly(dialkyldimethylammonium chloride) (PDDA, M_w = 200 000–350 000, 20 wt%) and 1H, 1H, 2H, 2H-perfluorooctyltriethoxysilane (POTS) was purchased from Sigma Aldrich. The concentration of PDDA aqueous solution used in all the experiments was 2 mg mL^{-1}. Aqueous ammonia (25%) and absolute ethanol (99.5%) were purchased from Beihua Fine Chemicals. Monodispersed SiO_2 NPs of ca. 25 nm (S-25), and ca.250 nm (S-250) were prepared according to the Stöber method.[40] For preparing 25 nm SiO_2 NPs, 3 mL TEOS was added dropwise to a flask containing a mixture of 5 mL aqueous ammonia, and 100 mL absolute ethanol under magnetic stirring. The reaction was carried out at 50 °C for 17 hours. For preparing 250 nm SiO_2 NPs, 3 mL TEOS was added dropwise to a flask containing a mixture of 7.5 mL aqueous ammonia, 100 mL absolute ethanol and 2 mL deionized water under magnetic stirring. The reaction was carried out at room temperature instead of elevated temperature for 17 hours. It is worth mentioning here that the as-prepared suspensions of 25 nm and 250 nm SiO_2 NPs had a pH value of ca. 10-11, and were used directly in the subsequent LBL self-assembling. The stainless steel meshes (pore size: 100 μm; wire

diameter: 60 μm) were purchased from the Sintered Filter Technic Co., Ltd., Shijiazhuang, China (SEM image was shown in Supporting information Figure S1). The sintered stainless steel fiber felts (filter precision: 5 μm) were purchased from the Xinxiang Lier Filter Technology Co. Ltd., Xinxiang, China. The pore size of the blank felt was measured by Quantachrome Porometer 3G through-pore size analyzer (10.1 μm, detail data in Figure 6). These stainless steel substrates were treated by ultrasonic cleaning in ethanol and deionized water before use.

LBL assembly of SiO_2 NPs coatings: The cleaned substrates were dipped alternatively in the PDDA solution (2 mg/mL) and the as-prepared suspensions (0.1 wt. %) of SiO_2 NPs of different particle sizes for 1 min under magnetic stirring for an appropriate number of cycles with the same operation procedures. The redundant polyelectrolytes (PDDA) in each cycle and SiO_2 NPs were removed by shaking the sample in pure water for 1 min, followed by drying it with flowing N_2. Finally, the as-prepared coatings were blown dry again with pure N_2 at room temperature.

Hydrophobic modification: The surface hydrophobic modification of the substrate assembled with SiO_2 NPs was carried out by simple chemical vapor deposition (CVD). The substrate was placed in a stainless steel autoclave with a Teflon container (100 mL), and a few droplets of POTS (5 μL) were dispensed to the bottom of the container. There was no direct contact between the substrate and the POTS droplets. The autoclave was then sealed and put in an oven at 120 ^{o}C for 1 h to enable the vapor of POTS to react with the hydroxyl groups of the substrate surface. Finally, the autoclave was opened, and placed in an oven for additional 2 h at 150 ^{o}C

to volatilize the unreacted POTS molecules on the substrate.

Oil/water separation: The commercial stainless steel mesh (felt) was used as the control, the hydrophobically treated stainless steel mesh (felt) and that with 3+1 SiO_2 NP coatings were used for oil/water mixture separation. In the following, n+m is used to denote n deposition cycles of 250 nm SiO_2 NPs and m deposition cycles of 25 nm SiO_2 NPs.

To study the oil/water separation performance of the materials mentioned above, two methods were used. One is the static membrane separation driven simply by gravity. A mixture of oil (n-hexadecane) and water (50 v/v %) was poured slowly into a filtering system where the filter mesh was placed in the middle with proper seals as shown in Figure 5a. The water phase was colored with methylene blue for easy observation. No external pressure was applied to drive the liquid through the filter. The other method used the filter as an oil coalescer is shown in Figure 7a. Surfactant-free emulsion was prepared by mixing water and n-hexadecane using a homogenizer running at 15000 rpm for 10 min. The initial n-hexadecane concentration in the emulsion was controlled at 1000 ppm. The droplet size of the emulsion was in the range of 1-20 μm as observed by optical microscopy (see Figure S6 in supporting information). Immediately after it was prepared, the emulsion was put into a syringe, hand-pushed steadily through the filter holder 25 mm in diameter. The oil droplets passing through the filter were coalesced and the filtrate was collected in the sample bottle. An instant clear filtrate indicates good separation; the oil separated will be on top of the sample due to the density difference of oil and

water. Quantitative separation efficiency was calculated using the remaining oil content in water analyzed with an Oil 460 Infrared photometer oil content analyzer from the Beijing China Invent Instrument Tech. Co. Ltd., Beijing, China.

Characterization: For transmission electron microscopy (TEM) experiments, powder samples were put on carbon-coated copper grids, and observed on a JEOL JEM-2100F transmission electron microscope at an acceleration voltage of 200 kV. Freshly fabricated coatings were examined by scanning electron microscopy (SEM) on a Hitachi S-6700 scanning electron microscope operated at 10 kV. For surface component analysis, a BRUKER-VECTOR22 FT-IR microscope was used to collect attenuated total reflection infrared (ATR-IR) spectra. Water and oil contact angle (WCA) of the different surfaces was measured at ambient temperature on a contact angle/interface system (DSA100, KRÜSS GmbH), where 4 μL liquid volume was used for proper observation if not otherwise indicated. AFM was conducted on an Agilent 5500 AFM/SPM microscope. The oil-in-water emulsion size was observed with an optical microscopy (6XB-PC) made by Shanghai optical instrument factory.

3. Results and Discussion

3.1. Synthesis of Super-hydrophobic Hierarchical SiO_2 NP Coatings

The substrate surface of stainless steel mesh or felt was firstly modified with positive charges by electrostatically adsorbing PDDA. Since the point of zero charge (PZC) is 2.1 for SiO_2,[41] the surface of SiO_2 NPs is negatively charged at pH 10. Therefore, when the substrate with a layer of PDDA was dipped into the suspension

of SiO_2 NPs, the particles were deposited on the substrate surface quickly by electrostatic interaction. The scanning electron microscopy (SEM) images in Figure S1 and S2 (see in the Supporting Information) show the blank stainless steel mesh and the mesh adsorbed with 250 nm SiO_2 NPs, respectively. The deposition is a uniform single particle layer; it does not block the mesh pores. The number of particles adsorbed on the surface by two deposition cycles of PDDA/SiO_2 NPs (Figure S2c, d) increases compared with a single deposition cycle (Figure S2a, b). That is to say by controlling the number of deposition cycles, the SiO_2 NP coating coverage and the surface roughness can be easily manipulated,[42] which is an important precondition for further tuning the surface wettability.

In order to increase the roughness, we deposited the 250 nm SiO_2 NPs on the stainless steel mesh a few times first, then assembled the 25 nm SiO_2 NPs on the substrate just once. For convenience, here we use 1+1, 2+1, and 3+1 to indicate the coatings as one, two and three deposition cycles of bigger particles followed by just one deposition cycle of the smaller particles, respectively. The SEM images in Figure 1 show the morphology of the mesh surfaces with 1+1, 2+1, and 3+1 coatings thus prepared. It can be seen that the particles are uniformly assembled on the wire surface, and the particle coverage increases with increasing deposition cycles of 250 nm SiO_2 NPs. Interestingly, after further assembly of small SiO_2 NPs on the surface of large SiO_2 NPs, hierarchal structure like raspberry fruit is formed (Figure 1b, d, f). The 1+1, 2+1, and 3+1 coatings were further hydrophobically treated by CVD method described previously.[35] Compared with the original assembly coatings of 1+1, 2+1,

and 3+1 (Figure 1b,d,f), the coatings undergone hydrophobic modification do not change much in terms of their surface morphology and retention of the hierarchical structure (Figure 2c,d,e), indicating a very thin hydrophobic perfluoroalkylsilane (POTS) layer of coverage. For comparison, SEM images in Figure 2a, and 2b also respectively give the morphology of the smooth surface of the blank mesh with hydrophobic modification only, and the mesh uniformly assembled with 25 nm SiO_2 NPs. Overall, it is noted that the hierarchically structured coatings constructed by SiO_2 NPs with two distinct sizes (250 nm vs. 25nm) have more nano-scaled ups and downs, which increases the roughness of the mesh surface. We also conducted the atomic force microscopy (AFM) experiments on the blank mesh without any modification and the mesh with 3+1 coatings plus hydrophobic modification (Figure S3 in the Supporting Information). The observed topography agrees with those observed in the SEM images (Figure 2a and 2e), and the root-mean-square (RMS) roughness (Ra) increases from 5.5 (Figure S3a) to 18.5 nm (Figure S3c). Figure S4 in supporting information shows the attenuated total reflection infrared (ATR-IR) spectra of the blank stainless steel mesh (a), the meshes with 3+1 coatings before (b) and after (c) hydrophobic treatment. The additional peaks at 2926 cm^{-1} and 2856 cm^{-1} for the hydrophobically modified mesh are the methylene asymmetry and symmetry peaks of POTS, a proof of successful chemical treatment. The 2300~2400 cm^{-1} peaks are attributed to CO_2 present in air.

3.2. Wetting Properties

As is well known, the Young's equation (Equation 1) is based on the assumption

of an ideal plane.

$$\cos\theta = \frac{\gamma_{SV} - \gamma_{SL}}{\gamma_{LV}} \quad (1)$$

where $\gamma_{SV,}$ γ_{SL} and γ_{LV} are the interfacial tensions of solid-air, solid-water and water-air interfaces, respectively. However, it does not apply to the rough surface coated with particles as described here. .

The Wenzel (Equation 2) and Cassie-Baxter equations (Equation 3) further developed the wetting theory by introducing the roughness factor.

$$\cos\theta' = r\cos\theta \quad (2)$$

$$\cos\theta' = f\cos\theta + f - 1 \quad (3)$$

where θ is the static contact angle on a smooth surface, θ' is the apparent contact angle on a rough surface, r is the Wenzel roughness factor, and f is the Cassie roughness factor defined as the fraction of the solid area in contact with the liquid droplet divided by both the solid and the hollow areas under the droplet. When the surface wetting situation suits Wenzel model, the apparent contact angle will increase with increasing r for hydrophobic materials. When the surface wetting situation suits Cassie model, the apparent contact angle will increase with the f factor decreasing. The roughened surface makes r to increase for Wenzel wetting model and f to decrease for Cassis wetting model. Thus the surfaces with particle coatings we prepared have high contact angle (the upper right inset images in Figure 2c, d, e). It was found that with increasing coating coverage of the 250 nm particles, the water contact angle (WCA) of the surfaces increase from 133 ^{o} (1+1 coatings with hydrophobic modification) to 143^{o} (2+1 coatings with hydrophobic modification), and

further to 158° of super-hydrophobicity (3+1 coatings with hydrophobic modification). Table 1 lists all the contact angle data of the above surfaces. The volume of all droplets used is 4μL. It is interesting to see that the oil (n-hexadecane) contact angle (OCA) follows the same trend as water (Figure 3). As shown in Figure 3, the hydrophobic modification decreases the surface energy of stainless steel, thus the contact angel increases from 80° (Figure 3a) to 124° (Figure 3d). However, the smooth surface with hydrophobic modification cannot reach super-hydrophobicity requiring WCA to be over 150°. When the surface roughness is increased using nanoparticle deposition, the contact angle increases to 158°. This is due to, as expected, the existence of air trapped in the hierarchically structured coatings in micro/nano scale that prevents water from further penetrating to the inner surfaces. The surface of the 3+1 coatings with hydrophobic modification not only shows super-hydrophobicity, but also very low sliding angle. 10 μL water droplet can easy roll down this surface with a tilt angle of 5° , and the rolling velocity is 290.4 mm/s (Figure 3j,k,l). The oil contact angles (OCAs) of the blank mesh and the mesh with hydrophobic modification are 38° and 101° (Figure 3b and 3e). However, the OCA does not increase significantly among the 1+1, 2+1 and 3+1 coated surfaces. They are 107°, 111° and 115° respectively (Table 1). As it was noticed, these contact angle data agreed qualitatively with the wetting theories developed for the solid-liquid-air interfaces only. For solid-oil-water interfaces, the wetting behavior of oil on an ideal smooth solid surface under water can be described by Equation 4, as deduced by Jung and Bhushan,[43] via combining the Young's equation at solid-water-air interface and

solid-air-oil interface.

$$\cos\theta_{OW} = \frac{\gamma_{OV}\cos\theta_O - \gamma_{WV}\cos\theta_W}{\gamma_{OW}} \quad (4)$$

where θ_{OW} is the oil contact angle, γ_{OV}, γ_{WV} and γ_{OW} are the interfacial tension of oil-air, water-air and oil-water interfaces, respectively. θ_W and θ_O are the WCA and OCA in air. According to this equation, hydrophilic surface (θ_W <90°) will show underwater oleophobicity (cos θ_{OW} <0). For a hydrophobic (θ_W >90°) yet oleophilic (θ_O<90°) surface in air, it will always be oleophilic underwater (cos θ_{OW} >0). For a hydrophobic but oleophobic surface, if γ_{OV} cos θ_O > γ_{WV} cos θ_W, an oleophilic surface property will be observed underwater (cos θ_{OW} >0), otherwise an oleophobic property will be seen (cos θ_{OW} <0). The underwater OCAs for the blank stainless steel mesh, the mesh with hydrophobic modification and the mesh with 3+1 coatings plus hydroohobic modification were measured to be 120° , 98° and 78° (Figure 3c,f and i) . For the hydrophilic blank mesh, it is apparent that its underwater oleophobicity agrees qualitatively with Equation 4's prediction. In our experiment, the oil is n-hexadecane so γ_{OV} is 25 mN/m. γ_{WV} is 73 mN/m and γ_{OW} is 53 mN/m, so the calculated OCAs underwater are 82°, 48° and 0° for the blank stainless steel mesh, the mesh with hydrophobic modification and the mesh with the 3+1 coatings plus hydrophobic modification, respectively. The predicted data do not agree with the experimental data because of the complex surface roughness effect, which is not predictable by any means so far. The results also suggest that equation 4 has many rooms to be modified to account for other surface geometric factors.

3.3. Oil/water Separation

In view of the contrary wettability of water and oil on the particle coated hydrophobic mesh, it is expected that these two liquids have different permeability towards the mesh. In order to prove this, we first conducted the static separation of unstirred regular oil/water mixture.

3.3.1. Mesh Performance

As shown in Figure 4a, we poured a mixture of n-hexadecane and water colored with methylene blue (50 v/v%) to the mesh holder (2.5 cm in diameter) fixed between two fixtures. The oil passed through the surperhydrophobic mesh with 3+1 coatingss into the beaker, driven simply by gravity, while water was repelled and kept in the upper glass measuring tube. No visible water leaked to the collecting bottle under the filter. In addition, the 35 ml separated water were held stable above the superhydrophobic mesh with the 3+1 particle coatings (HPM) over 1 h, and the maximum holding time was 3 h 24 min. On contrast, the hydrophobic chemically treated only mesh (HM) could merely retain water for 2 min. The blank mesh as the control (M) did not retain water at all so no oil/water separation was observed. The penetration pressure, or rather the hydrostatic head, is an important indicator for the mesh's ability to separate oil and water. Water does not pass through the mesh below the pressure. The maximum height of water column (h_{max}) the mesh filter can support is equivalent to the penetration pressure (P) that can be mutually converted using the following equation:

$$P = \rho g h_{\max} \quad (5)$$

Where ρ is the density of water and g is the acceleration of gravity. As shown in

Figure 4b, the average penetration pressure of HPM for three measurements is 1.1±0.04 kPa, corresponding to a maximum support height of 11.3±0.43 cm. As a comparison, the penetration pressure of HM and M are 0.83±0.03 kPa and 0 kPa.

The separation efficiency, as interpreted here by the water rejection coefficient (R%), can be calculated as follows:

$$R(\%) = \left(1 - \frac{V_p}{V_0}\right) \times 100 \qquad (6)$$

where V_0 and V_p are the water volume in the original oil/water mixture and that in the collected oil after the separation. As is shown in Figure 4c, the separation efficiency of HPM is around 99.5% every time in 20 times of repeated tests, indicating the material's stable surface property. Figure S5 also shows the water contact angles (WCAs) on the mesh with both particle coatings and hydrophobic modification after the coated surfaces are immersed in soybean oil and hydrochloric acid solution (pH 4.02) for 120 h. The WCAs are 154 °and 148.4° respectively after immersion in oil and acid solution, compared with its original value of 158°. This indicates the coating is relatively robust, especially in oil. However, its resistance to acid could be a concern that merits further improvement.

3.3.2. Fiber Felt Performance

The performance of oil/water separation for the aforementioned mesh relies not only on the mesh's water repellency and oil affinity, but also on the mesh hole size. The mesh with smaller hole size can be used to separate dispersed water from oil more effectively by sieving mechanism, which is a different subject. Our goal is to separate emulsified oil from water by not designing a surface filtration media that

necessitates the surface oleophobicity and hydrophilicity about which much other work is concerned. Considering the need of pumping a very large amount of water through the filter for separating a small amount of dispersed oil, the mesh is designed to be used as an oil coalescer instead of an oil stripper. As such, we mixed oil (hexadecane) with water using a homogenizer to form an oil-in-water emulsion and tested its separability using the different materials intentionally designed. The filter with SiO_2 NP coatings and hydrophobic modification worked better than other materials when the emulsion was forced through the filtering mesh using a peristaltic pump, but with low separation efficiency. The reason is that the stainless steel mesh (mesh size 100 μm) does not have enough depth and the right pore size to work as an effective coalescer to separate an emulsion sizing 1-20 μm (Figure S6 in supporting information). For a coalescer, which is a depth filter, water and oil are driven through the depth of the media all together. Smaller oil droplets are firstly transported into the filter and attached to the fiber surfaces prior to combining and deforming through the filter media subject to water shear forces. Grown oil droplets will release more easily followed by floating up from the downstream side of the media, where separation is accomplished by the density difference of oil and water. Highly efficient coalescing will enable the formation of larger oil droplets much faster. As it is well known, filter media made with fibers are good choices for depth filtration. [44] Therefore，we selected a sintered stainless steel fiber felt as the substrate to fabricate the particle coated hydrophobic coalescence media, using the same procedure described previously. SEM image in Figure 5 shows the fiber surface morphology. Clearly SiO_2 NPs were

assembled on the fiber surface and the hierarchical structure was seen as well even through a few layers of fibers into the felt. As Figure 5a shows, the maximum surface pore size can be around a hundred micrometers, but the through pore size of the multi-layered felt is much smaller because of the overlaps of the stainless steel fibers. The mean pore size of the felt was measured with a capillary flow porometer and results are shown in Figure 6 [10.4 μm for the blank felt as the control, 9.0 μm for the felt modified with hydrophobic modification (HP) only, and 7.8 μm for the felt with 2+1 particle coatings plus hydrophobic modification (HPF)] Interestingly, the HPF has bi-mode pore size distribution, and the smaller average pore size compared its counterparts implies partial pore blocking due to the existence of particles.. Nonetheless, this felt exhibits oleophilicity under water, its dynamic oil contact angle became zero in 3 seconds after initial contact (Figure S7 in the Supporting Information) and it also performs well for oil-in-water emulsion separation. In our experiments, 50 ml (1000 ppm) oil-in-water emulsion were put in a syringe and pushed through the filter mounted in a holder as shown in Figure 7a. The collected liquid passing through HPF is clear, the one through HF is translucent, and the one through F is as turbid as the original emulsion, as is shown in Figure 7b (videos are in the Supporting Information). The oil concentrations of emulsions after the separation were measured by infrared photometer oil content analyzer. Table 2 shows the results, an average of three filtration experiments. The oil/water separation efficiency is calculated using Eq.7:

$$R_o=(1-C_p/C_0)*100\% \qquad (7)$$

where C_p is the oil concentration of filtrate and C_0 is the original oil concentration (1000 ppm). The measurement showed that the oil/water emulsion separation efficiency of the bare felt (F) is only 28.3%. Surprisingly, the efficiency of HF is as good as 98.4%. The efficiency of HPF is the highest (99.4%) and the oil concentration in the filtrate is lowered to 6.5 ppm. We kept challenging the HPF felt and repeatedly used it for 20 times for the same filtration, and found that the filtration efficiency remained at 99.2%, an indication of good stability and durability of the coatings thus prepared. The surface composition of the coating was measured by XPS before and after the material was used 20 times for oil/water separation, and the results are shown in Figure S8. The F 1s peak was clearly observed, indicating the persistent existence of the modifying agent POTS. The 1% efficiency difference between HF and HPF merits some discussion. The former has a slightly larger average pore size, which tends to lower the separation efficiency as a coalescer if challenged by the same size emulsion. The question arising here immediately is if the surface wettability matters for the coalescence separation. As observed in the experiments, the bare felt has superoleophilicity under water. An oil droplet generated from a needle under water was sucked into the felt in no time on contact, no surface spreading ever occurred. For HP and HFP surfaces, initial oil spreading was observed before the droplet went into the materials. In fact, it took 5 and 3 seconds for the oil droplet to completely wiggle into HF and HPF respectively. That is to say HPF is less wettable by oil under water than HF. We speculate that the reason the felt (F) failed to separate the emulsion is its relatively larger pore size and hydrophilicity that allow the emulsion to go right

through without oil being captured. The superoleophilicity observed is magnified by the big pore size. HF and HPF were treated with hydrophobicity toward oleophobicity in air, so when the emulsion was forced through the material, in some sense water gave way to oil to preferably adsorb on the fiber surface for coalescence to effectively take place. So surface wettability does matter. However, it is difficult to find the balance point between pore size and wettability so the 1% efficiency difference for HF and HPF is believed to be a result of a dual effect of both. Further work is being conducted to optimize the coatings to address issues like this and many others.

4. Conclusions

A series of SiO_2 NP coatings with raspberry-like micro/nanostructure and hierarchical roughness were successfully constructed on stainless steel mesh and stainless steel fiber felt. This was achieved via facile LBL self-assembly of SiO_2 NPs with different sizes. The resultant mesh after hydrophobic chemical treatment exhibits superhydrophobicity, thus can efficiently separate oil and water by letting oil through and water repelled. Moreover, the felts with such NP coatings and chemical treatment can also separate oil-in-water emulsion with efficiency over 99% and long durability for continuous use. This is important for applying the material in a harsh environment such as oil and gas field produced water treatment, where robustness and long-service life are necessary,

Acknowledgements. This work was supported by the Chinese Academy of Sciences under the talented program.

References

1. A. B. Nordvik, J. L.Simmons, K. R. Bitting, A. Lewis and T. Strom-Kristiansen, *Spill Sci. Technol. Bull.* 1996, **3**, 107-122.

2. X. Gui, J. Wei, K. Wang, A. Cao, H. Zhu, Y. Jia, Q. Shu and D. Wu, *Adv. Mater.* 2010, **22**, 617-621.

3. A. K. Kota, G. Kwon, W. Choi, J. M. Mabry and A. Tuteja, *Nat. commun.* 2012, **3**, 1025.

4. R. Wahi, L. A. Chuah, T. S. Y. Choong, Z. Ngaini and M. M. Nourouzi, *Sep. Purif. Technol.* 2013, **113**, 51-63.

5. A. Fakhru'l-Razi, A. Pendashteh, L. C. Abdullah, D. R. A. Biak, S. S. Madaeni and Z. Z. Abidin, *J. Hazard Mater.* 2009, **170**, 530-551.

6. M. Santander, R. T. Rodrigues and J. Rubio, *Colloids Surf., A* 2011, **375**, 237-244.

7. L. Zhang, Y. Zhong, D. Cha and P. Wang, *Sci. Rep.* 2013, **3**, 2326.

8. T. R. Annunciado, T. H. D.Sydenstricker and S. C. Amico, *Mar. Pollut. Bull.* 2005, **50**, 1340-1346.

9. D. Angelova, I. Uzunov, S. Uzunova, A. Gigova and L. Minchev, *Chem. Eng. J.* 2011, **172**, 306-311.

10. Y. Zhu, F. Zhang, D. Wang, X. F. Pei, W. Zhang and J. Jin, *J. Mater. Chem. A* 2013, **1**, 5758-5765.

11. W. Zhang, Y. Zhu, X. Liu, D. Wang, J. Li, L. Jiang and J. Jin, *Angew. Chem. Int. Ed. Engl.* 2014, **53**, 856-860.

12. W. Zhang, Z. Shi, F. Zhang, X. Liu, J. Jin and L. Jiang, *Adv. Mater.* 2013, **25**, 2071-2076.

13. Z. Shi, W. Zhang, F. Zhang, X. Liu, D. Wang, J. Jin and L. Jiang, *Adv. Mater.* 2013, **25**, 2422-2427.

14. D. Vasanth, G. Pugazhenthi and R. Uppaluri, *Desalination* 2013, **320**, 86-95.

15. D. Wandera, H. H. Himstedt, M. Marroquin, S. R. Wickramasinghe and S. M. Husson, *J. Membrane Sci.* 2012, **403-404**, 250-260.

16. L. P. Wen, Y. Tian, J. Ma, J. Zhai and L. Jiang, *Phys. Chem. Chem. Phys.* 2012, **14**, 4027-4042.

17. X. Yao, Y. Song and L. Jiang, *Adv. Mater.* 2011, **23**, 719-734.

18. C. Gao, Z.Sun, K. Li, Y. Chen, Y. Cao, S. Zhang and L. Feng, *Energ. Environ. Sci.* 2013, **6**, 1147-1151.

19. W. Liang and Z. Guo, *RSC Advances* 2013, **3**, 16469-16474.

20. S. J. Maguire-Boyle and A. R. Barron, *J. Membrane Sci.* 2011, **382**, 107-115.

21. B. Wang and Z. Guo, *Chem. Commun.* 2013, **49**, 9416-9418.

22. C. R. Crick, J. A. Gibbins and I. P. Parkin, *J. Mater. Chem. A* 2013, **1**, 5943-5948.

23. J. Zhang and S. Seeger, *Adv. Funct. Mater.*, 2011, **21**, 4699-4704.

24. A. Li, H.-X. Sun, D.-Z. Tan, W.-J. Fan, S.-H. Wen, X.-J. Qing, G.-X. Li, S.-Y. Li and W.-Q. Deng, *Energ. Environ. Sci.*, 2011, **4**, 2062-2065.

25. L. Wu, J. P. Zhang, B. C. Li and A. Q. Wang, *J. Mater. Chem. B* 2013, **1**, 4756-4763.

26. G. Caputo, B. Cortese, C. Nobile, M. Salerno, R. Cingolani, G. Gigli, P. D. Cozzoli and A. Athanassiou, *Adv. Funct. Mater.* 2009, **19**, 1149-1157.

27. M. Zhang, C. Wang, S. Wang, Y. Shi and J. Li, *Appl. Surf. Sci.* 2012, **261**, 764-769.

28. P. A. Levkin, F. Svec and J. M. Fréchet, *Adv. Funct. Mater.* 2009, **19**, 1993-1998.

29. Q. F. Xu, J. N. Wang and K. D. Sanderson, *ACS Nano* 2010, **4**, 2201-2209.

30. S. Li, H. Xie, S. Zhang and X. Wang, *Chem. Commun.* 2007, 4857-4859.

31. H. Yang, P. Pi, Z.-Q. Cai, X. Wen, X. Wang, J. Cheng and Z.-r. Yang, *Appl. Surf. Sci.* 2010, **256**, 4095–4102.

32. X. Du and J. He, *ACS Appl. Mater. Inter.* 2011, **3**, 1269-1276.

33. B. Wang and Z. Guo, *Appl. Phys. Lett.* 2013, **103**, 063704.

34. J. Zimmermann, F. A. Reifler, G. Fortunato, L.-C. Gerhardt and S. Seeger, *Adv. Funct. Mater.* 2008, **18**, 3662-3669.

35. X. Li, J. He and W. Liu, *Mater. Res. Bull.* 2013, **48**, 2522-2528.

36. X. Li and J. He, *ACS Appl. Mat. Interfaces* 2013, **5**, 5282-5290.

37. B. Zhao and M. M. Collinson, *Chem. Mater.* 2010, **22**, 4312-4319.

38. X. Du, X. Li and J. He, *ACS Appl. Mat. Interfaces* 2010, **2**, 2365-2372.

39. X. Li, X. Du and J. He, *Langmuir* 2010, **26**, 13528-13534.

40. W. Stöber, A. Fink and E. Bohn, *Colloid Interface Sci.* **1968**, *26*, 62-69.

41. X. Zhang, O. Sato, M. Taguchi, Y. Einaga, T. Murakami and A. Fujishima, *Chem. Mater.* **2005**, *17*, 696-700.

42. X. Li and J. He, *ACS Appl. Mat. Interfaces* **2012**, *4*, 2204-2211.

43. B. Bhushan, Y. C.Jung and K. Koch, *Langmuir* **2009**, *25*, 3240-3248.

44. M. A. Abdullah, A. U. Rahmah and Z. Man, *J Hazard Mater.* **2010**, *177*, 683-691.

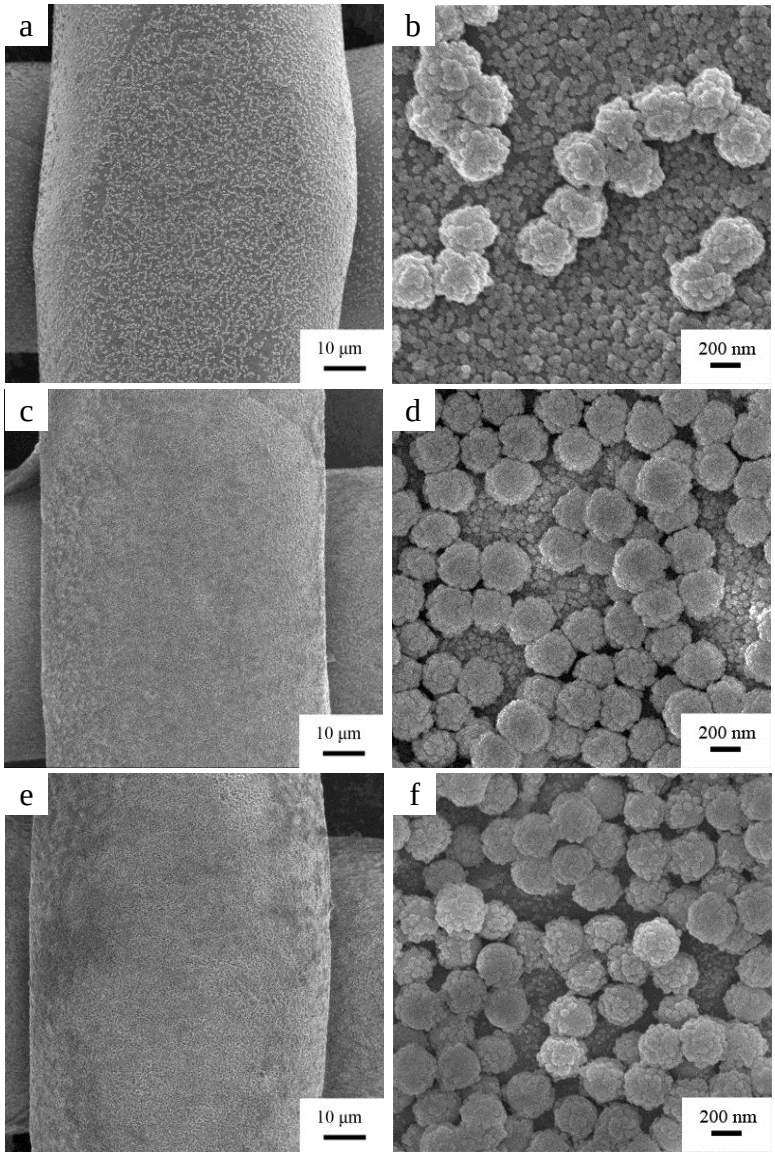

Figure 1. SEM images of mesh surface with particle coatings obtained by 1+1 (a,b), 2+1 (c,d), and 3+1 (e,f) deposition before hydrophobic modification (n+m is used to denote n deposition cycles of 250 nm nanoparticles and m deposition cycles of 25 nm SiO_2 nanoparticles bilayer).

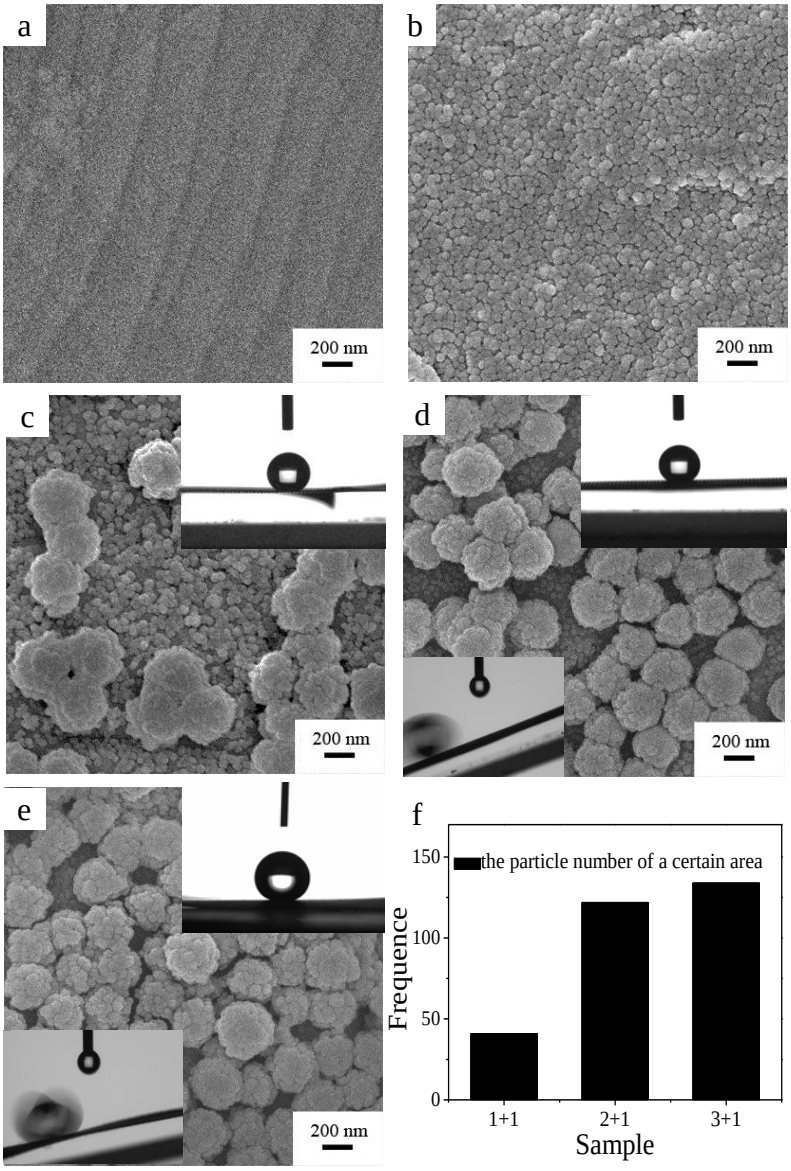

Figure 2. SEM images of the blank mesh surface without any particle coatings but with chemical hydrophobic modification (a) and mesh surface with particle coatings obtained by two deposition cycles of 25 nm SiO_2 nanoparticles (b), 1+1 (c), 2+1 (d), and 3+1 (e) deposition plus hydrophobic modification (n+m is used to denote n deposition cycles of 250 nm nanoparticles and m deposition cycles of 25 nm SiO_2 nanoparticles). (f) Histograms of particle density on the mesh surface with particle coatings obtained by 1+1 (c), 2+1 (d), and 3+1 (e) deposition plus hydrophobic modification. The upper right insets in (a-e) are the digital images of WCA on the corresponding mesh surfaces. The lower left insets in (d,e) are the digital images of sliding angles on the corresponding mesh surfaces.

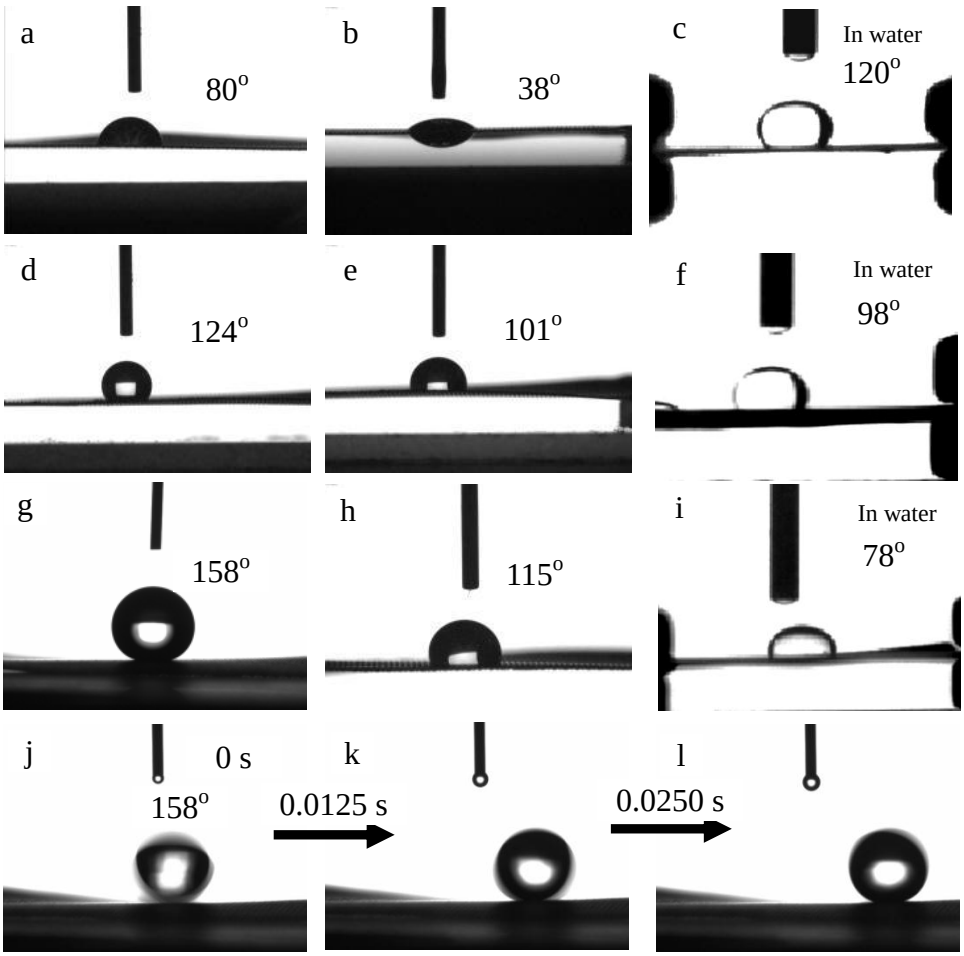

Figure 3. Digital images of water contact angle on blank mesh in air (a), the mesh with hydrophobic modification (d) and the mesh with 3+1 coatings plus hydrophobic modification (g); the corresponding oil contact angle in air (b,e,h) and under water (the image was flipped over for the convenience of angle measurement) (c,f,i), respectively. The n-hexadecane was used as the oil. The volume of the droplet used is 4 μL. The successive digital images (j,k,l) of the dynamic movement of a 10 μL water droplet on the mesh with 3+1 coatings and hydrophobic modification (sliding angle SA=5°).

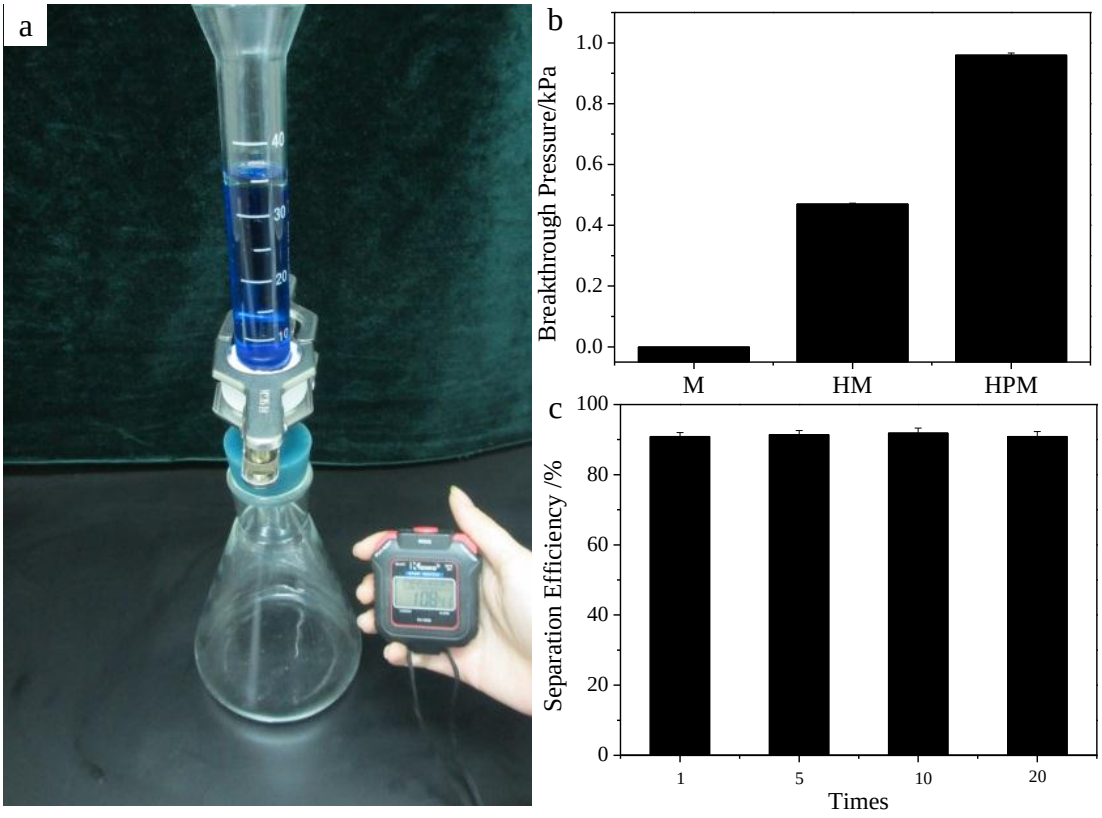

Figure 4. (a) Digital image of the mesh with 3+1 coatings and hydrophobic modification used as a filter mounted and sealed in between the white parts of system. It can retain 35 ml water (dyed by methylene blue) for more than 1 h, and maximum 3 h 24 min; while the mesh without particle coatings but with hydrophobic modification can only retain the same amount of water for 1 min 58 s. (b) Breakthrough pressure of stainless steel mesh (M), hydrophobic mesh (HM) and hydrophobic particle-coated mesh (HPM). (c) Separation efficiency and durability performance of hydrophobic particle-coated mesh (shortened as HPM-n. HPM-20 indicates that the separation efficiency remains even after 20-time re-uses for oil/water separation. n-hexadecane is the oil.).

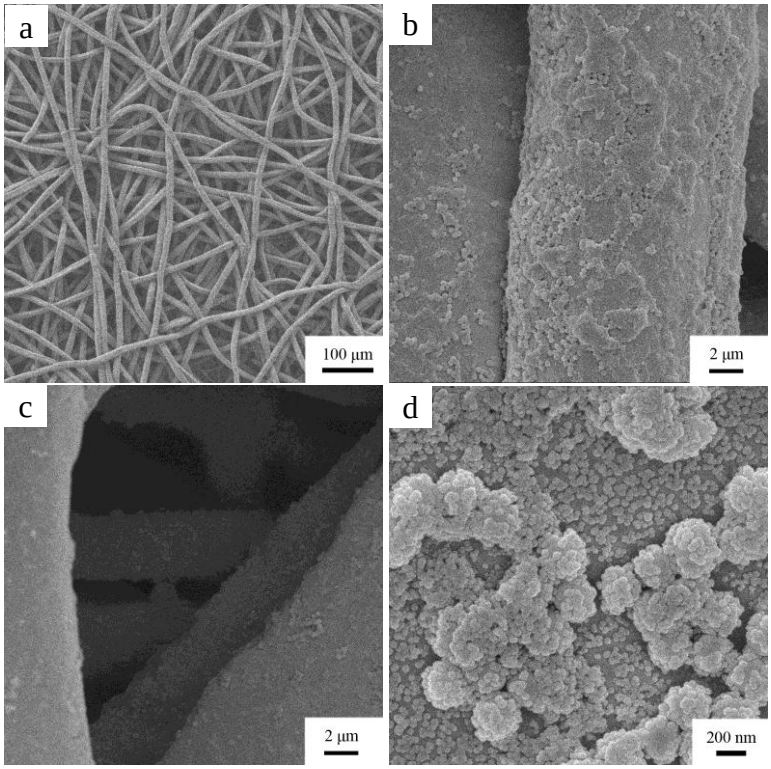

Figure 5. SEM images (a-d) of stainless steel fiber felt with 2+1 particle coatings.

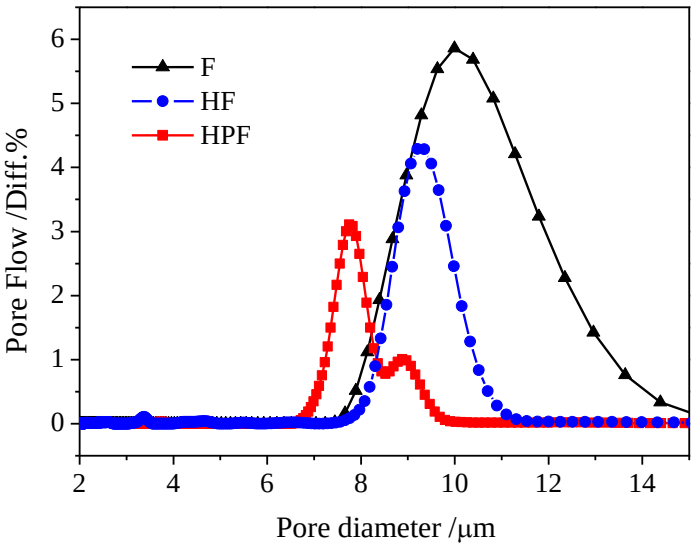

Figure 6. Pore size distribution of the blank felt as control (F), felt with hydrophobic modification (HF) only, and felt with particle coatings plus hydrophobic modification (HPF).

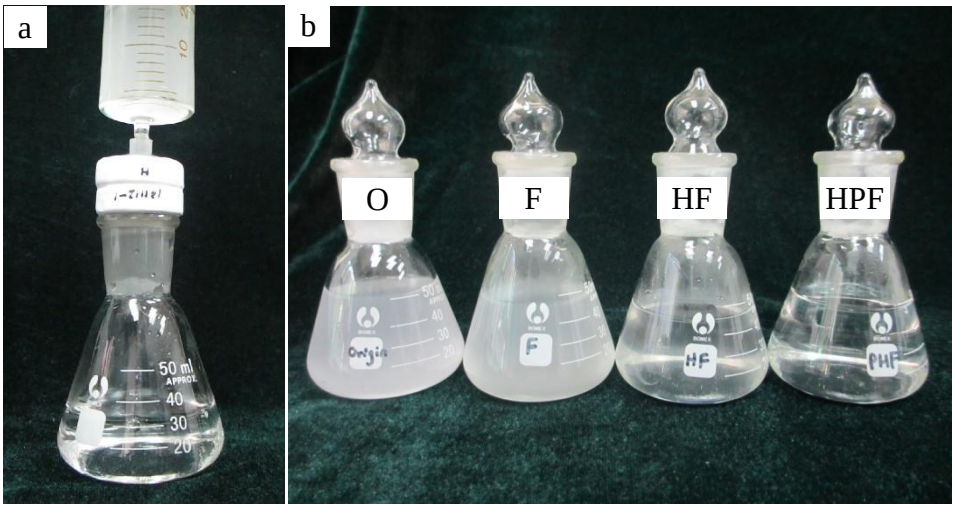

Figure 7. (a) Digital image of an oil-in-water emulsion being pushed through the stainless steel fiber felt mounted and sealed in between the white parts of the system. The felt is used as a coalescence media for oil droplets. (b) Images of the original 1000 ppm emulsion (O), the emulsion filtered by the felt as control (F), the emulsion filtered by the felt with hydrophobic modification (HF), and the emulsion filtered by the felt with both particle coatings and hydrophobic modification (HPF).

Table 1. Water and oil contact angle of different materials prepared.

	The blank mesh	The mesh with hydrophobic modification	The mesh with 1+1 coatings and hydrophobic modification	The mesh with 2+1 coatings and hydrophobic modification	The mesh 3+1 coatings and hydrophobic modification
Water contact angle (WCA)	80°	124°	133°	143°	158°
Oil contact angle (OCA)	38°	101°	107°	111°	115°

1+1, 2+1, and 3+1 indicate the coatings as one, two and three deposition cycles of bigger particles (250 nm SiO_2 NPs) followed by just one deposition cycle of the smaller particles (25 nm SiO_2 NPs), respectively.

Table 2. Oil-in-water emulsion separation data for different materials. The oil concentration of the original emulsion is 1000 ppm. The n-hexadecane is used as the oil. The results shown here are averages of three individual experiments.

	The blank felt as control (F)	The felt with hydrophobic modification (HF)	The felt with particle coatings and hydrophobic modification (HPF)	HPF after 20 times separation experiments
Oil concentration /ppm	717.1	16.2	6.5	7.8
Oil/water separation	28.3%	98.4%	99.4%	99.2%